# Electronic Supplementary Information

## Silk-Derived Carbon Nanosheets for Transparent Conducting Electrodes on Flexible Substrates

Se Youn Cho,[a,b] Moataz Abdulhafez,[a] Golnaz Najaf Tomaraei,[a] Jaegeun Lee,[a,c] and Mostafa Bedewy*[a,d,e]

[a] *Department of Industrial Engineering, University of Pittsburgh, Pittsburgh, Pennsylvania 15261, United States*

[b] *RAMP Convergence Research Center, Korea Institute of Science and Technology, 92 Chudong-ro, Bongdong-eup, Wanju-gun, Jeonbuk 55324, Republic of Korea*

[c] *School of Chemical Engineering, Pusan National University, Busan 46241, Republic of Korea*

[d] *Department of Mechanical Engineering and Materials Science, University of Pittsburgh, Pittsburgh, Pennsylvania 15261, United States*

[e] *Department of Chemical and Petroleum Engineering, University of Pittsburgh, Pittsburgh, Pennsylvania 15261, United States*

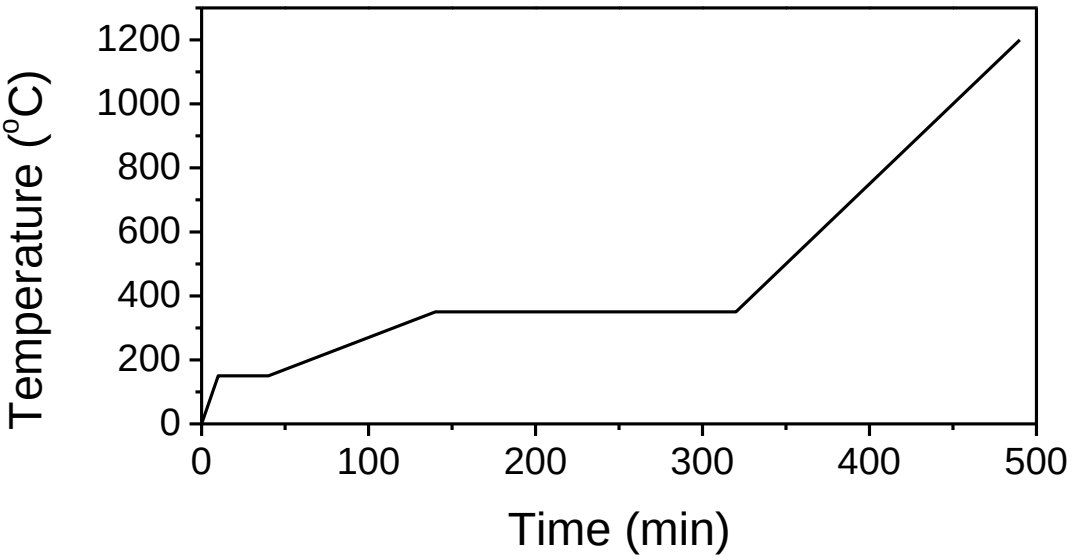


**Figure S1.** Temperature schedule of carbonization process for silk fibroin-based carbon nanosheets.

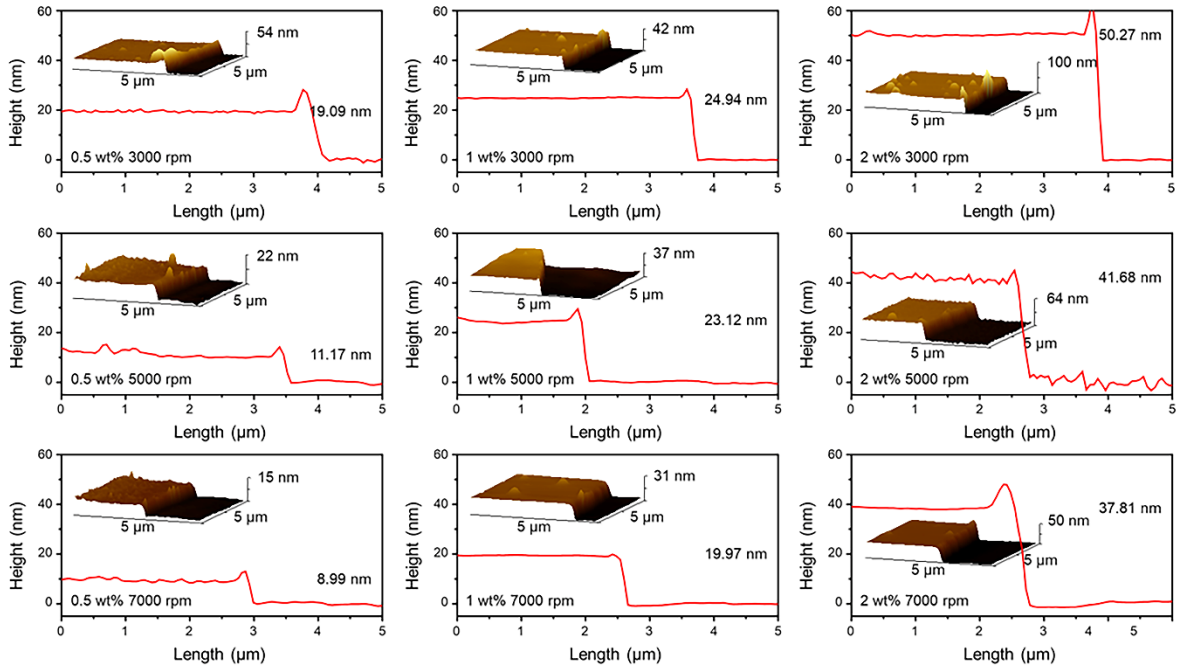


**Figure S2.** AFM images showing thickness dependence of the silk fibroin thin film on the spin rates and the concentrations of silk fibroin.

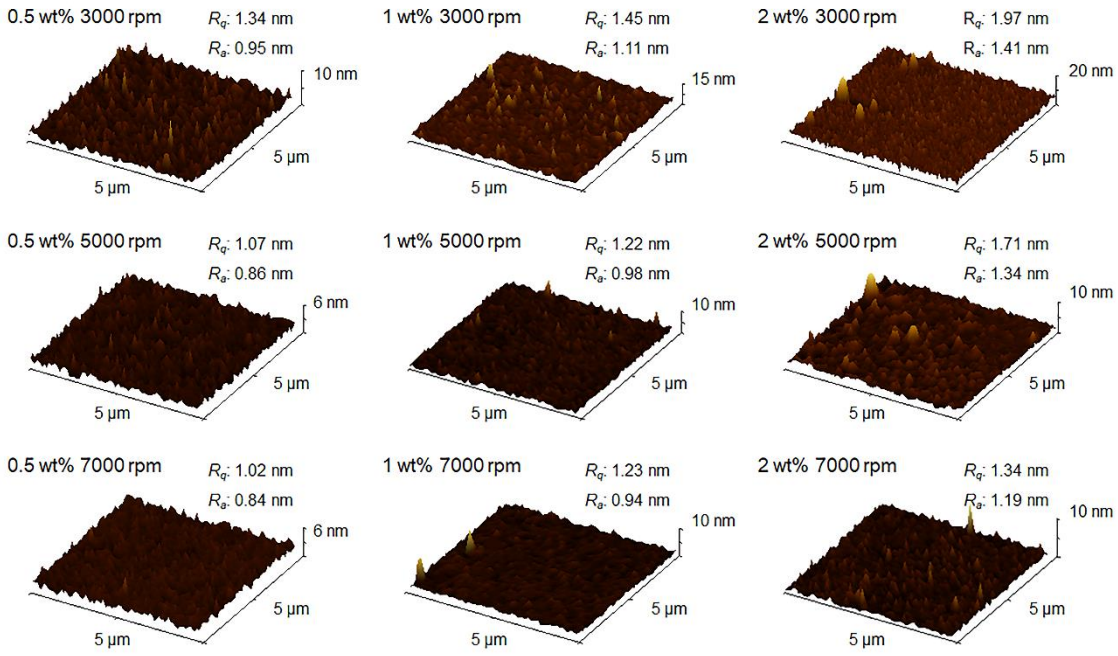


**Figure S3.** 3D AFM topography images showing the surface roughness of silk fibroin films prepared at different solution concentrations (0.5–2.0 wt.%) and spin-coating speeds (1000–7000 rpm). Ra values correspond to 5 × 5 µm scan areas on $SiO_2$/Si substrates.

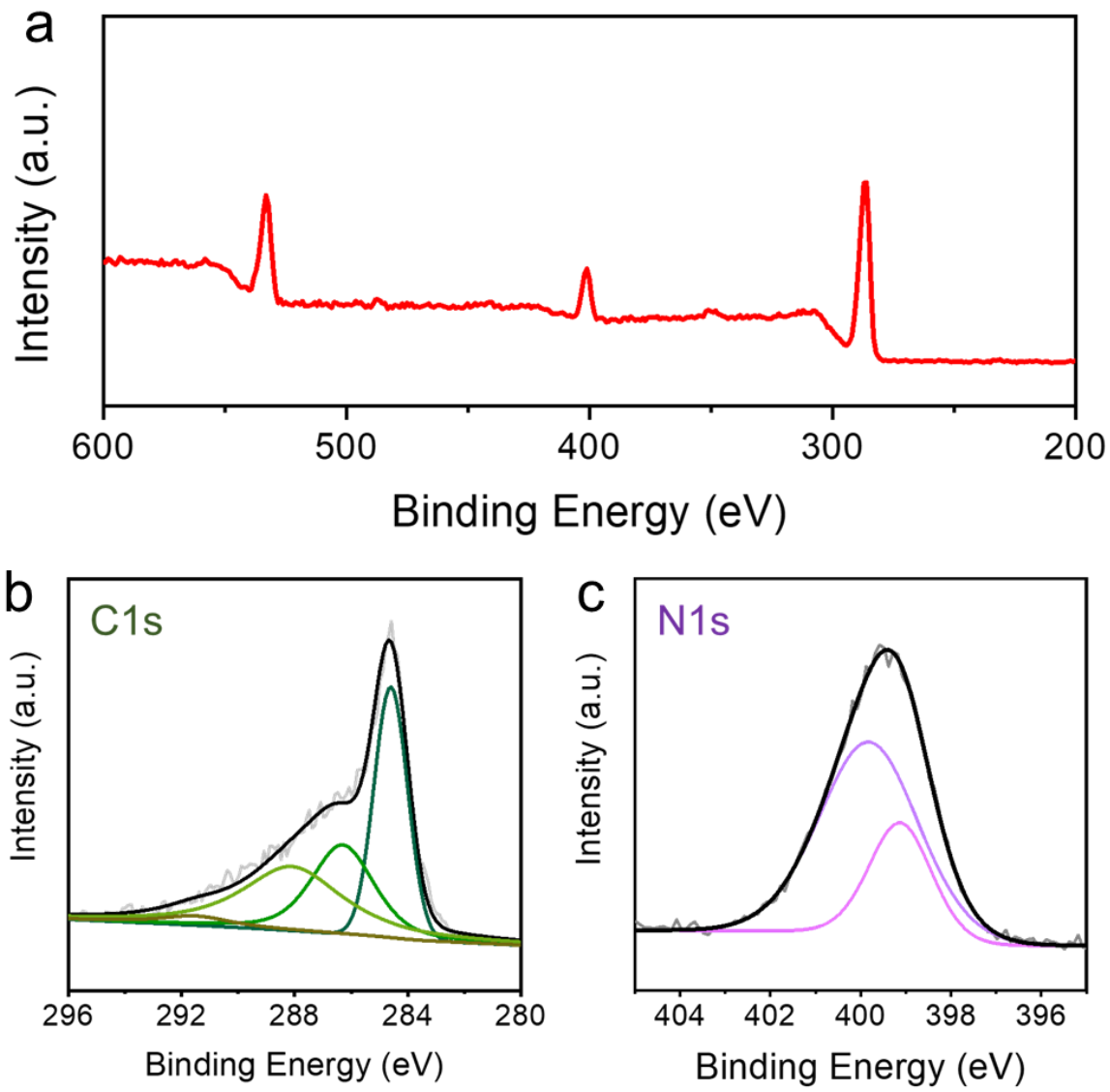


**Figure S4.** (a) XPS survey spectra of regenerated silk fibroin, and deconvoluted high-resolution spectra of (b) C1s and (c) N1s.

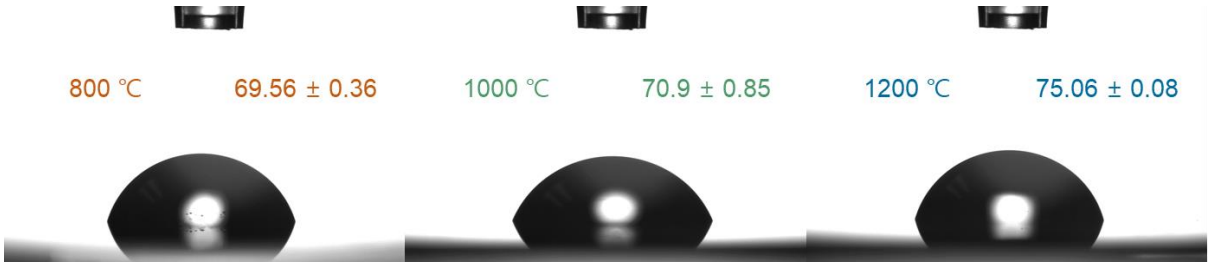


**Figure S5**. Contact angle of a water droplet on the surface of silk fibroin-derived carbon nanosheets prepared with different temperature.

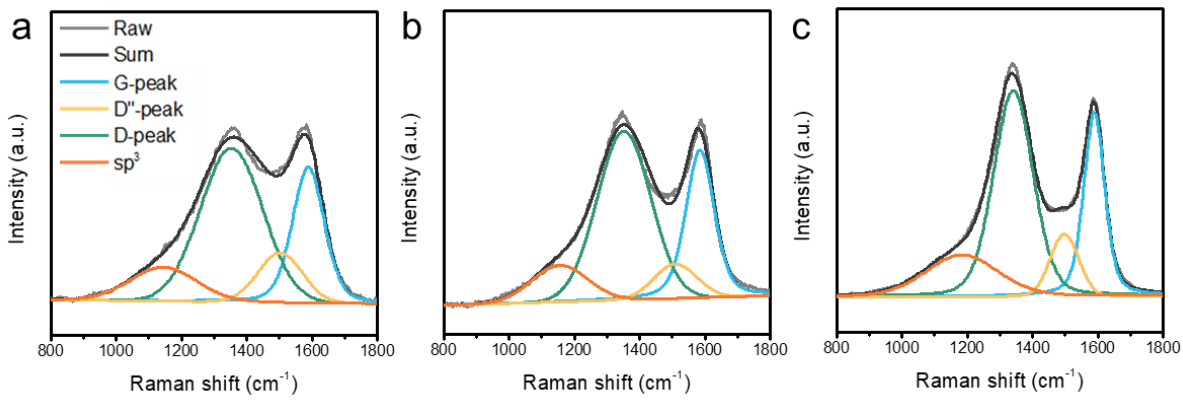


**Figure S6.** Deconvolved Raman spectra of SF-derived carbon nanosheets heat-treated at (a) 800 ºC, (b) 1,000 ºC, and (c) 1,200 ºC.

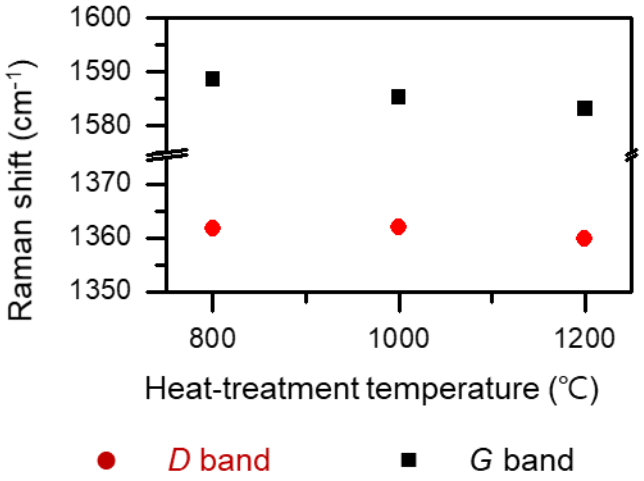


**Figure S7**. Position of *D* and *G* bands of silk fibroin-based CNs according to heat-treatment temperature.

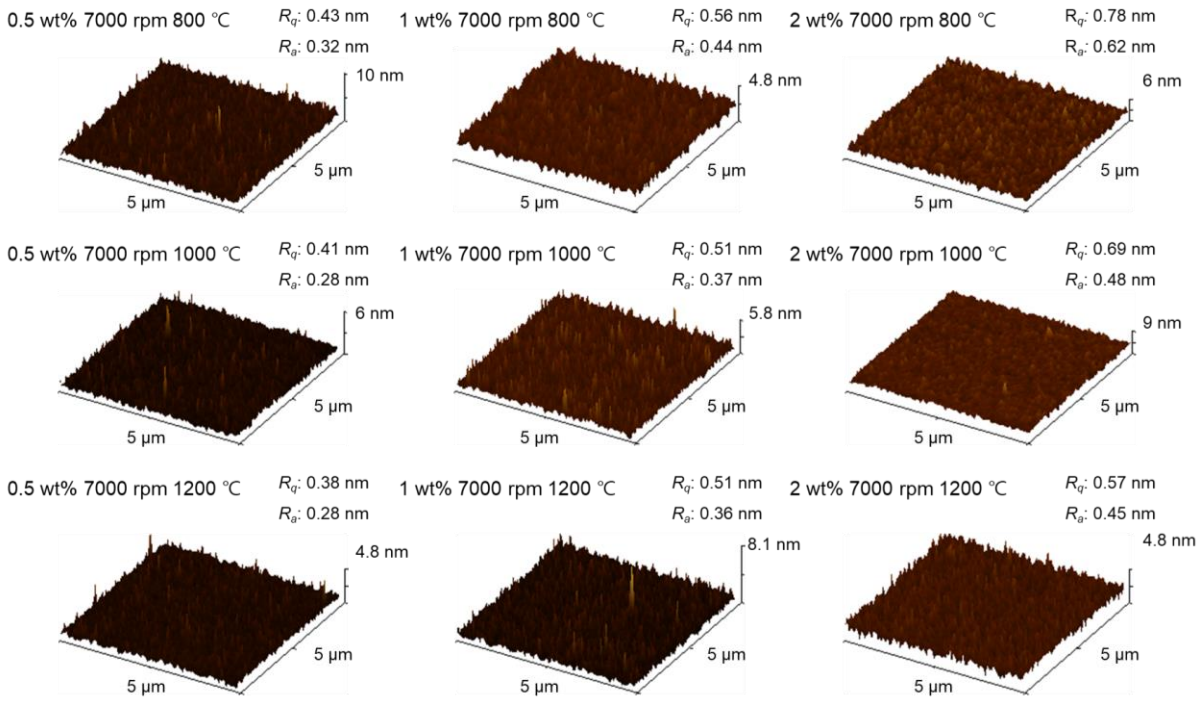


**Figure S8.** Surface roughness of silk fibroin-derived carbon nanosheet films with different concentration and HTT.

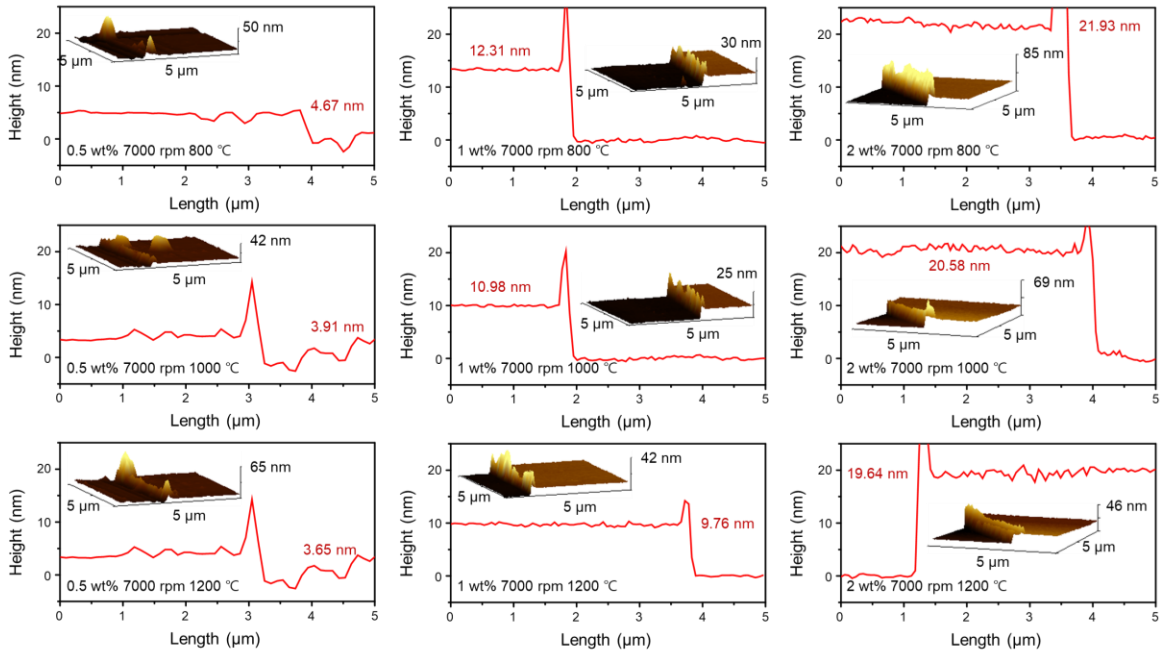


**Figure S9.** AFM images and thickness of carbonized silk fibroin thin films prepared using different concentration and HTT

**Table S1.** Elemental composition and chemical structure of regenerated SF by XPS Analysis

| Element | Binding Energy | Assignment | Atomic Fraction by XPS | Atomic Fraction by theoretical Calculation* |
|---|---|---|---|---|
| | 284.6 eV | C-C, C-H | | |
| C 1s | 285.9 eV | C-N | 0.64 | 0.55 |
| | 288.2 eV | O=C-N | | |
| O 1s | 531.0 eV | O in amide | 0.21 | 0.24 |
| N 1s | 398.50 eV | N in amide | 0.15 | 0.21 |

*Data calculated from the 10 main amino acid residue (Gly, Ala, Ser, Try, Val, Asp/Asn, Thr Glu/Gln, Phe, and Iie) known as comprising 98.1% of the total composition of silk fibroin

**Table S1.** Comparison of representative carbon-based transparent conductive films, including graphene-, CNT-, and polymer-derived carbon nanosheets, highlighting their transmittance at 550 nm and sheet resistance values

| Material | Transmittance @ 550 nm (%) | Sheet Resistance (Ω/sq) | Ref. |
|---|---|---|---|
| single-layer graphene film | 89.0~96.5 | 300~11200 | S1 |
| bilayer graphene film | 83.0~94.7 | 180~500 | S1 |
| graphene/polymer nanocomposite | >90 | ~15 | S2 |
| carbon-welded SWCNT | >90 | 41 | S3 |
| CNT–PAA hybrid | 91/84 | 150/60 | S4 |
| polyimide-derived CNSs | 54~89 | 1600~14700 | S5 |
| polyethylene-derived CNSs | 80~90 | $10^2$~$10^3$ | S6 |
| Nitrogen-containing oligomers | | 100-2000 | S7 |
| PAN-derived CNSs | 80~90 | $10^2$~$10^3$ | S8 |
| CNS from silk (this work) | >98 | ~ $10^2$ | This work |

**References**

S1. S. Lee, K. Lee, C. H. Liu, and Z. Zhong, Nanoscale, 2012, 4(2), 639-644.

S2. C. Biswas, I. Candan, Y. Alaskar, H. Qasem, W. Zhang, A. Z. Stieg, Y.-H. Xiw, and K. L. Wang, Sci. rep., 2018, 8, 10259.

S3. S. Jiang, P. X. Hou, M. L. Chen, B. W. Wang, D. M. Sun, D. M. Tang, Q. Jin, Q.-X. Guo, D.-D. Zhang, K.-P. Tai, J. Tan, E. O. Kauppinen, C. Lui, and H.-M. Cheng, Sci. adv., 2018, 4(5), eaap9264.

S4. Y. Zhou, R. Azumi, and S. Shimada, Nanoscale, 2019, 11(9), 3804-3813.

S5. G. Souri, S. J. Yu, H. Yeo, M. Goh, J.-Y. Hwang, S. M. Kim, B.-C. Ku, Y. G. Jeong, and N.-H. You, RSC Adv., 2016, 6(58), 52509-52517.

S6. M. Yi, M. Han, J. Chen, Z. Hao, Y. Chen, Y. Yao, and R. Sun, Nanomaterials, 2021, 12(1), 111.

S7. K. K. Chung, N. Fechler, M. Patrini, P. Galinetto, D. Comoretto, and M. Antonietti, Carbon, 1015, 94, 1044-1051.

S8. S. I. Na, Y. J. Noh, S. Y. Son, T. W. Kim, S. S. Kim, S. Lee, and H. I. Joh, Appl. Phys. Lett., 2013, 102(4).